


# Linear and nonlinear kinetic Alfvén waves at Venus

A. A. Fayad<sup>1</sup> , W. M. Moslem<sup>2,3</sup>, H. Fichtner<sup>1</sup>, and M. Lazar<sup>1,4</sup>

<sup>1</sup> Institut für Theoretische Physik IV, Ruhr-Universität Bochum, 44780 Bochum, Germany  
e-mail: [fayadhalaa@gmail.com](mailto:fayadhalaa@gmail.com); [Alaa.Fayad@ruhr-uni-bochum.de](mailto:Alaa.Fayad@ruhr-uni-bochum.de)

<sup>2</sup> Department of Physics, Faculty of Science, Port Said University, Port Said 42521, Egypt

<sup>3</sup> Centre for Theoretical Physics, The British University in Egypt (BUE), El-Shorouk City, Cairo, Egypt

<sup>4</sup> Centre for mathematical Plasma Astrophysics, Department of Mathematics, KU Leuven, Celestijnenlaan 200B, 3001 Leuven, Belgium

Received 7 December 2022 / Accepted 18 May 2023

## ABSTRACT

Space observations show that Venus suffers significant atmospheric erosion caused by the solar wind forcing. Plasma acceleration is found to be one of the main mechanisms contributing to the global atmospheric loss at Venus through its magnetotail. Motivated by these observations, we propose that kinetic Alfvén waves (KAW) may be a possible candidate for charged particle energization at the upper atmosphere of Venus. To test this hypothesis, we explored the basic features of both linear and nonlinear KAW structures at Venus. We considered a low-but-finite  $\beta$  plasma consisting of ionospheric populations (consisting of hydrogen  $H^+$ , oxygen  $O^+$ , and isothermal ionospheric electrons) and solar wind populations (protons and isothermal electrons). In the linear regime, we obtain a linear dispersion relation that exhibits a dependence on the intrinsic plasma configuration at Venus. The linear analysis predicts wave structures with wavelengths of  $\sim 10\text{--}10^2$  km and frequencies of up to  $\sim 5$  Hz. In the nonlinear regime, small-but-finite-amplitude solitary excitations with their corresponding bipolar electric field are obtained through the reductive perturbation technique. We discuss the influence of the intrinsic plasma parameters (the ionic concentration, solar wind electron temperature, magnetic field strength, and obliqueness) on the nature of the structures of the solitary KAWs and their corresponding electric field. We find that the ambipolar field is amplified with increasing propagation angle, magnetic field strength, and relative temperature of electrons. Our theoretical analysis predicts the propagation of elliptically polarized ultra-low-frequency (ULF) solitary structures with a maximum magnitude of  $\sim 0.01\text{--}0.034$  mV m<sup>-1</sup> and a time duration of 20–30 s. The result of the fast Fourier transform (FFT) power spectra of the ambipolar parallel electric field is broadband electromagnetic noise in the frequency range of  $\sim 0.5\text{--}2$  Hz.

**Key words.** hydrodynamics – plasmas – waves – solar wind – planets and satellites: terrestrial planets

## 1. Introduction

At Venus, atmospheric material is continuously scavenged by the solar wind, leading to significant atmospheric erosion. The atmospheric escape issue is one of the most important processes for understanding the evolution of planetary atmospheres. There are various mechanisms that are responsible for the escape of planetary particles, and these processes are crucially dependent on the type of interaction pattern of the celestial objects with the solar wind. Celestial objects may be planets, moons/satellites, comets, and asteroids. For instance, particle escape depends on many different factors, such as the object's proximity to the Sun, and its resilience against solar wind forcing, the activity of the Sun, the object's magnetic shielding, and gravity (Lundin 2011). There are two main groups of escape mechanisms, namely thermal escape; which is concerned with neutral atmospheric particles, and nonthermal escape; which is mostly concerned with charged planetary particles. Nonthermal escape includes different mechanisms such as the photo-chemical reaction, atmospheric sputtering, and plasma acceleration. Particle escape from Venus was reported by the two long-term missions, Pioneer Venus Orbiter (PVO; Colin 1980) and Venus Express (VEX; Titov et al. 2006; Svedhem et al. 2007), which were devoted to exploring the Venusian plasma environment and its interaction with the solar wind. Observational data suggest that plasma acceleration is primarily responsible for all of the escape and

outflow of ionospheric plasma at Venus (Lundin 2011; Futaana et al. 2017). There are many categories of plasma acceleration, including particle–particle interaction, wave–particle interaction, and field-aligned electric fields (Lundin 2011; Pérez-de Tejada & Lundin 2023). In other words, planetary ions may be accelerated by the convection of electric and magnetic fields related to the solar wind (Coates 2004), or by the plasma waves propagating in the Venusian environment. Ionic escape has been discussed for many years and in several works (see e.g., Terada et al. 2004; Jarvinen et al. 2009, 2016; Dubinin et al. 2011; Salem et al. 2020; Moslem et al. 2021).

In tenuous plasmas, such as space and astrophysical plasmas, collisions are rare. Therefore, conversion of energy and momentum happens indirectly via wave forcing. One interesting wave phenomenon is the kinetic Alfvén wave (KAW), which plays a vital role in energy and charge transport within space plasmas by virtue of its quasi-electrostatic nature (Cramer 2011); that is, the wave sustains two electric field components: the parallel component is electrostatic and the perpendicular component is inductive. Waves involving only purely electrostatic electric fields are called electrostatic waves (e.g., ion-acoustic waves and Langmuir waves), while waves involving inductive electric fields are called electromagnetic waves (e.g., compressional Alfvén waves). Quasi-electrostatic waves include both components, and support the transport, heating, and acceleration of particles, and may contribute to the atmospheric loss process. This behavior

appears in Alfvén waves as a result of the contribution of the kinetic effects (due to a finite Larmor radius or finite inertial length effects) to the dynamics of the wave. The KAW is a modified mode of the well-known magnetohydrodynamic (MHD) nondispersive Alfvén waves, where they attain a dispersive character as a consequence of oblique propagation with respect to the local magnetic field along with the contribution of kinetic effects. KAWs are hybrid waves that are noncompressive for low propagation angles  $\theta$  (e.g., electromagnetic ion cyclotron (EMIC) waves propagating quasi-parallel to the magnetic field) and compressive for highly oblique angles, when KAWs develop a large longitudinal electric field (along  $\mathbf{k}$ ), such that the electric field becomes primarily electrostatic (Gary 1986). KAWs are known to be elliptically polarized, in contrast to the linearly polarized ideal MHD Alfvén waves (Cramer 2011). Furthermore, the dispersion of the KAWs can interplay with the nonlinear steepening effect to form nonlinear localized structures called solitary kinetic Alfvén waves (SKAWs; Hasegawa & Mima 1976). SKAWs are found to form spiky regions associated with plasma-density depletion with enhanced electric fields and parallel currents (Seyler et al. 1995). Terrestrial observations show that the plasma environment in which these waves are observed is usually characterized by density gradients, transversely accelerated ions, and field-aligned accelerated electrons (Wahlund et al. 1994; Stasiewicz et al. 1997; Knudsen & Wahlund 1998). Other observations from the FAST spacecraft have reported that erosion of the ionospheric plasmas from the topside ionosphere is caused by the action of dispersive Alfvén waves (Chaston et al. 2006).

A superthermal ionospheric population above and within the Venusian ionopause (~500–2000 km) was detected by PVO and its ion mass spectrometer (OIMS; Taylor et al. 1980a; see Taylor Jr et al. 1980b; Grebowsky et al. 1993) and neutral mass spectrometer (ONMS; see Kasprzak et al. 1982). Various mechanisms have been suggested for the generation of these superthermal populations. For example, Taylor Jr et al. (1981) suggested turbulent acceleration of planetary ions at the lower boundary of the magnetosheath. Alternatively, Curtis et al. (1981) proposed that acceleration of ions is accomplished by an electric field parallel to the ambient magnetic field at the ionopause: The large-scale shear (greater than the ionic gyroradius) produced by the parallel ionosheath flow relative to the ionopause generates MHD waves at the ionopause. The source of the electric field is the conversion of the Kelvin-Helmholtz-driven MHD surface wave to a shear Alfvén wave with an electric field component parallel to the ambient magnetic field. This parallel electric field accelerates the planetary ions to energies comparable to those observed by the ONMS over a region comparable in size to the ion gyroradius. The accelerated ions follow the draped magnetic field around the planet in an anti-sunward direction. Kasprzak et al. (1982) suggested that ions are accelerated out of the ionosphere by the shocked solar wind through plasma wave–particle interaction. Szegő et al. (1991) claims that electrostatic waves can be excited through the relative drift of the cold ionospheric ions to the magnetosheath plasma; the waves then propagate down to the ionosphere to heat and accelerate both the electrons and ions to superthermal energies.

Owing to the dynamical behavior of the transition zone at Venus, and the occurrence of the energetic ion signature above the ionopause (Taylor Jr et al. 1980b; Grebowsky et al. 1993), we anticipate the presence of kinetic Alfvénic solitary excitations in the upper Venusian atmosphere. Moreover, we think these excitations may play a role as an energization mechanism that is responsible for the superthermal populations found above the

ionopause and may contribute to the atmospheric escape process by accelerating particles along the field lines. The electric field of the solitary excitations is known to be bipolar in nature; consequently, bipolar structures are usually considered as a fingerprint of solitary waves. However, localized bipolar electric field structures have not yet been reported at the Venusian transition region. This may be due to a lack of suitable instrumentation on the previous space missions that visited Venus. Confirmation of the presence of these waves may help to provide an explanation as to the heating and acceleration processes that happen above the ionopause. Therefore, to provide insights into the features of these excitations for future missions, we use the observational data reported by PVO and VEX of the plasma configurations at the transition zone at Venus (Lundin et al. 2011; Knudsen et al. 2016) and adopt a hydrodynamic formalism to explore the dynamics of both linear and nonlinear KAWs excited through the interaction of the solar wind with Venus. The plasma model relevant to the Venusian transition zone comprises two positive planetary species, namely hydrogen  $\text{H}^+$  and oxygen  $\text{O}^+$ , as well as isothermal planetary electrons, solar wind protons  $\text{H}^+$ , and isothermally distributed solar wind electrons.

This manuscript is divided into four sections. In Sect. 2, we introduce our hypothesis in more detail along with its mathematical treatment. We also present a linear analysis where the dispersion relation is obtained for harmonic waves. For the nonlinear regime, a Korteweg-de Vries (KdV) evolution equation is obtained for small-but-finite-amplitude kinetic Alfvénic solitary structures. In Sect. 3, we present and discuss our numerical evaluation of the bipolar electrostatic structures associated with the solitary KAWs. The main conclusions of the present study are outlined in Sect. 4.

## 2. Problem formulation

### 2.1. Physical representation

The solar wind and solar irradiance are interacting with the atmosphere of Venus to form various plasma boundaries, such as the ionosphere, the mantle, the magnetosheath, and the bow shock. Each region has its own unique features, which are controlled by many agents, such as the solar activity, and both the electromagnetic environment and the physical features of the planet (Dubinin et al. 2020). When the solar radiation heats and ionizes the atmospheric particles, an ionized layer is formed. This layer is called the ionosphere and is located just above the neutral atmosphere; it extends to heights of ~300 km at the subsolar region and its extent increases in height with the solar zenith angle until it reaches 1000 km at the terminator (Phillips & McComas 1991). The uppermost region of the ionosphere is defined as the ionopause, and is a thin layer of a few tens of kilometers that is marked with a sharp decrease in electron density (Brace & Kliore 1991). This region separates the cold planetary particles found in the ionosphere from the hot shocked solar wind at the magnetosheath flow. The induced magnetosheath is formed due to the piling up of the interplanetary magnetic field (IMF) lines during the solar wind interaction with Venus (Phillips & McComas 1991; Futaana et al. 2017). There is a transition region characterized by the presence of a mixture of both the cold ionospheric and hot magnetosheath flows just above the ionopause and underneath the magnetosheath (Spennner et al. 1980; Martinecz et al. 2009). This region is known as the mantle. Figure 1 illustrates the different plasma boundaries at Venus and the location of the superthermal ion populations (Brace & Kliore 1991; Lundin 2011). The mixture

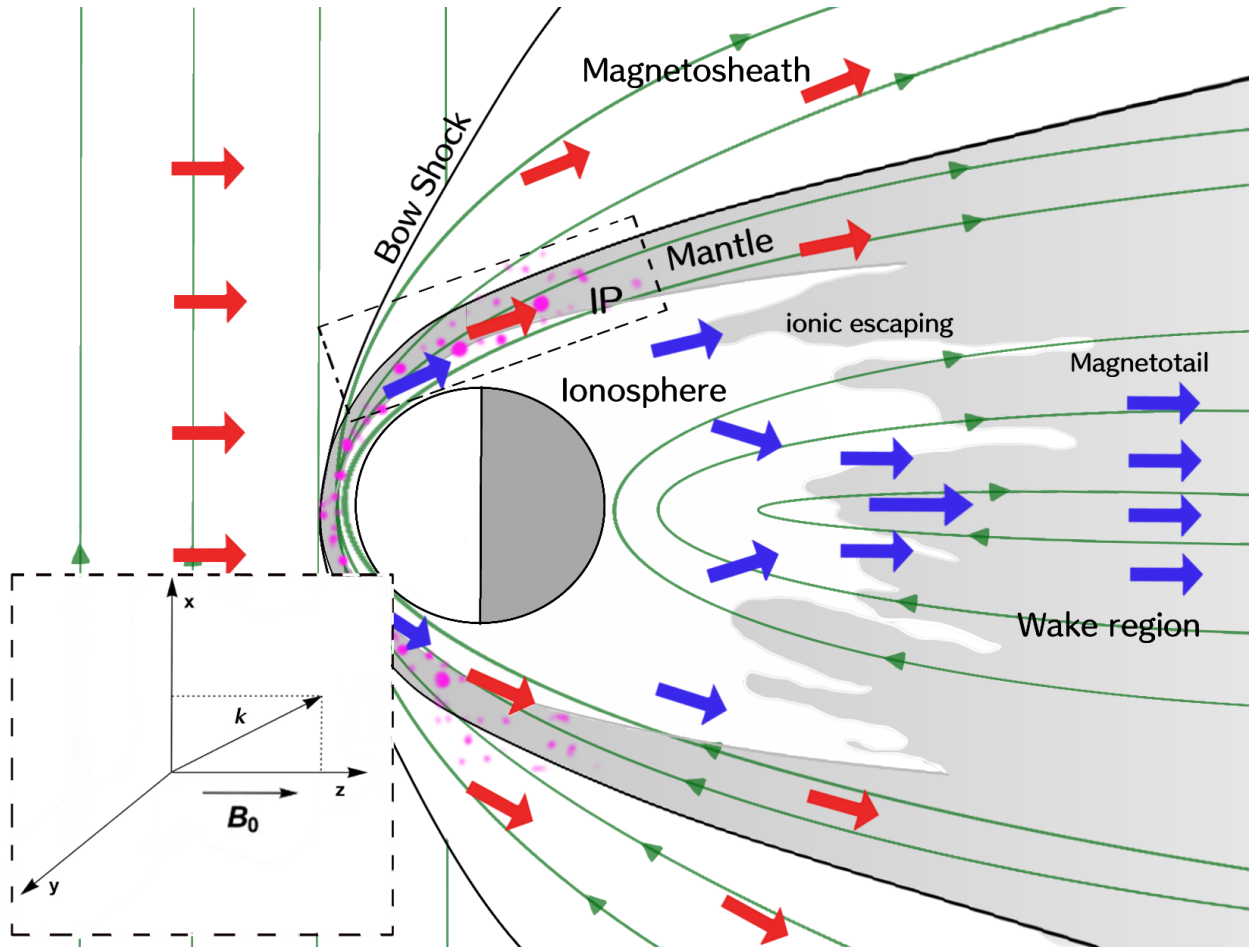


**Fig. 1.** Schematic representation of the plasma boundaries of Venus, indicating the flow of the solar wind (red arrows), the flow of the planetary ions (blue arrows), the interplanetary magnetic field lines (green), and the superthermal populations (magenta dots). For the region of interest (dashed rectangular), we show the wave geometry of the KAW and the orientation of  $\mathbf{k}$  and  $\mathbf{B}_0$  along the Cartesian coordinate system in the bottom left panel.

of the cold planetary ions with the hot solar wind flows provides a source of excess free energy to excite different instabilities and fluctuations. As mentioned above, many authors have suggested that the wave–particle interaction of these fluctuations can form the superthermal populations found in this region and can contribute to the escaping process.

In this work, we propose that dispersive Alfvén waves may contribute to atmospheric loss through accelerating particles along the draped field lines around Venus. Dispersive Alfvén waves have two distinct branches according to the plasma  $\beta$  (which is the ratio of the thermal pressure to the magnetic pressure), where different kinetic effects appear. Within the low- $\beta$  regime ( $\beta \ll m_e/m_i \ll 1$ ), a dispersive characteristic appears due to the finite electron inertial length. The waves of this branch are therefore called the “inertial Alfvén waves” (IAWs). While the other branch, namely the KAWs, appears because of the finite Larmor radius in low-but-finite  $\beta$  plasmas (i.e.,  $m_e/m_i \ll \beta \ll 1$ ; Baumjohann & Treumann 1996). Accordingly, we calculated the plasma  $\beta$  for the transition region parameters, that is, for the oxygen ion density  $n_O = 40 \text{ cm}^{-3}$ , the hydrogen ion density  $n_H = 15 \text{ cm}^{-3}$ , the solar wind proton density  $n_{sp} = 20 \text{ cm}^{-3}$ , the oxygen and hydrogen ion temperatures  $T_O = T_H = 0.2 \text{ eV}$ , the solar wind proton temperature  $T_{sp} = 20 \text{ eV}$ , and the local magnetic field strength  $B_0 = 80 \text{ nT}$  (Lundin et al. 2011; Knudsen et al. 2016). The plasma  $\beta = \sum_i k_B T_i n_i / (B_0^2 / 8\pi) \approx 0.032$ , which

falls in the low-but-finite  $\beta$  regime (where  $i$  stands for the  $i$ th ionic species and  $k_B$  is Boltzmann’s constant). Consequently, we expect the kinetic branch to exist in the transition region.

Kinetic Alfvén waves can accelerate particles in two ways: (1) the ions are either transversely accelerated by the perpendicular fields of the wave when  $\lambda_\perp \sim \rho_i$ , where  $\lambda_\perp$  is the perpendicular wavelength, and  $\rho_i$  is the ion Larmor radius; or (2) by the wave–particle interactions, where planetary particles can be accelerated through the parallel fields of the wave. At Venus, the magnetic field is draped around the planet and extends behind it to form the magnetotail. Thus, ions are usually accelerated or picked up by the solar wind electric fields along the field lines and then escape from the wake region (see Fig. 1). Therefore, we suppose that KAWs may be excited at the transition region and act as a possible particle energization candidate, thus contributing to the global atmospheric loss. The wave geometry along the Cartesian coordinate system is presented in Fig. 1.

## 2.2. Fluid model equations

We aim to study the dynamics and propagation properties of linear and nonlinear KAWs driven by the solar wind interaction with the ionospheric plasma of Venus. Based on observations, we consider a homogeneous, collisionless, magnetized, multi-component plasma model consisting of two ionospheric positive

ion species ( $H^+$  and  $O^+$ ), solar wind protons ( $sp^+$ ), inertialess ionospheric electrons ( $e^-$ ), and inertialess solar wind electrons ( $se^-$ ) (Afify et al. 2021). The ambient magnetic field is assumed to be directed along the  $z$ -axis, that is,  $\mathbf{B}_0 = B_0 \hat{z}$ , where  $\hat{z}$  is the unit vector along the  $z$ -axis. We assume that all the wave variations are in the  $x$ - $z$  plane, that is,  $(\partial_x, 0, \partial_z)$ , except the magnetic field perturbations, which have an induced component in the  $y$ -direction. Under the low-frequency assumption, that is,  $\omega \ll \Omega_i$  (where  $\Omega_i = eB_0/m_i c$  is the ion cyclotron frequency,  $e$ ,  $m_i$ , and  $c$  are the electron charge, the ion mass, and the speed of light, respectively) and in the low- $\beta$  plasma, the wave will produce no significant compression of the magnetic field,  $B_{z1} = 0$  (Cramer 2011). Moreover, in this case, we can use the two-potential theory (Kadomtsev 1956), where the electric field intensity along  $x$  and  $z$  directions is defined as follows:

$$E_x = -\partial_x \phi, \quad E_y = 0, \quad E_z = -\partial_z \psi, \quad (1)$$

where  $\phi$  and  $\psi (= \phi_{\parallel} + \int \partial_t A dz$ , where  $A$  is the vector potential) are defined as the electrostatic and electromagnetic potentials, respectively.

The continuity equation of the ionic species is given by

$$\partial_t n_i + \partial_x(n_i u_{ix}) = 0, \quad (2)$$

where  $i$  stands for  $O^+$ ,  $H^+$ , and  $sp^+$ . The ion fluid velocity perpendicular to the external magnetic field  $\mathbf{B}_0$  is given by (see Appendix B)

$$u_{ix} = -\frac{c}{B_0 \Omega_i} \partial_t \partial_x \phi, \quad (3)$$

which appears due to the polarization drift. The ion motion along the magnetic field is ignored here because we want to focus on the dynamics of the KAWs and avoid its coupling with the ion-acoustic waves. The continuity equation for electrons is given by

$$\partial_t n_j + \partial_z(n_j u_{jz}) = 0, \quad (4)$$

where  $j$  stands for  $e^-$ , and  $se^-$ . It should be noted that the parallel ion motion is neglected in the ion continuity Eq. (2), because the ion mass is much larger than that of electron, which causes the ion to have a larger Larmor radius, meaning that it spends most of the time in the perpendicular direction. On the other hand, the electron has a small mass and therefore a small Larmor radius and small polarization drift velocity, and so we can neglect its motion across the magnetic field. The ionospheric and solar wind electrons are both assumed to be inertialess and are therefore governed by the Boltzmann distribution:

$$n_e = n_{e0} \exp(e\psi/T_e), \quad (5)$$

$$n_{se} = n_{se0} \exp(e\psi/T_{se}), \quad (6)$$

where  $n_{e0}$  ( $T_e$ ) and  $n_{se0}$  ( $T_{se}$ ) correspond to the equilibrium density (temperature) of the ionospheric and solar wind electrons, respectively. The ionospheric and solar wind electron temperatures are defined in energy units. In the small-but-finite  $\beta$  plasma regime (i.e.,  $m_e/m_i \ll \beta \ll 1$ , where  $\beta$  is the ratio between the thermal pressure and the magnetic pressure), the thermal velocity of the electrons is much higher than the Alfvén velocity, and therefore electrons respond almost immediately to the electric potential of the wave, meaning their inertia can be neglected. Therefore, expressing the electron population densities using a

Boltzmann distribution is a valid approximation (Baumjohann & Treumann 1996).

Faraday's law  $\nabla \times \mathbf{E} = -\frac{1}{c} \partial_t \mathbf{B}$  for the two-potential theory can be expressed as

$$\partial_x \partial_z (\phi - \psi) = \frac{1}{c} \partial_t B_y. \quad (7)$$

Ampere's Law is expressed as

$$\nabla \times \mathbf{B} = \frac{4\pi}{c} \mathbf{J} + \frac{1}{c} \partial_t \mathbf{E}. \quad (8)$$

In the above equation, the contribution of the displacement current is neglected because of the low-frequency assumption  $\omega \ll \Omega_i$ , where the phase velocity of the wave is much lower than the speed of light. If we assume that  $\partial_t \sim t_{\text{char}}^{-1}$ , where  $t_{\text{char}}$  represents the characteristic timescale and  $\nabla \sim l_{\text{char}}^{-1}$ , where  $l_{\text{char}}$  is assumed to represent the corresponding characteristic length scale, the phase velocity  $V_{\text{ph}}$  is  $\sim l_{\text{char}}/t_{\text{char}}$ . Faraday's equation gives the scaling  $E/cB \sim V_{\text{ph}}/c$ . By comparing the magnitude of the displacement current to the left-hand side of Eq. (8), we see

that  $\frac{\partial_t \mathbf{E}}{c \nabla \times \mathbf{B}} \sim \frac{E/t_{\text{char}}}{cB/l_{\text{char}}} \sim \frac{V_{\text{ph}}^2}{c^2}$ . Subsequently, as  $V_{\text{ph}} \ll c$ , the displacement current term can be dropped from Ampere's law (Bellan 2008). In this case, we may write Eq. (8) as

$$\partial_x B_y = \frac{4\pi}{c} J_z. \quad (9)$$

The parallel current density  $J_z$  is entirely carried by electrons, where  $J_z = -en_e u_{ez} - en_{se} u_{sez}$ , where the first term represents the current density of the ionospheric electrons and the second is the current density of the solar wind electrons. Combining both Faraday's (7) and Ampere's laws (9), we have

$$\partial_x^2 \partial_z^2 (\phi - \psi) = \frac{4\pi}{c^2} \partial_t \partial_z J_z. \quad (10)$$

The current continuity equation  $\nabla \cdot \mathbf{J} = -\partial_t \rho = -\partial_t \sum n_\alpha q_\alpha$ , under the quasi-neutrality condition, that is,  $n_H + n_O + n_{sp} = n_{se} + n_e$ , is written as

$$\partial_x (J_{Ox} + J_{Hx} + J_{sp,x}) = -\partial_z (J_{ez} + J_{sez}), \quad (11)$$

where  $J_{Ox}$ ,  $J_{Hx}$ , and  $J_{sp,x}$  are the current densities of oxygen, hydrogen, and solar wind protons. We note here that the ion polarization drift  $u_{ix}$  provides the main contribution to the perpendicular current. This happens because ions have larger Larmor radii, which increases their motion perpendicular to the magnetic field. On the other hand, the parallel current is mainly dominated by the electrons because they are more free to move along magnetic field lines due their smaller Larmor radius than ions. It is important to note that we can use the quasi-neutrality condition because the assumed wave frequency is well below the electron plasma frequency, and the Debye length is assumed to be negligibly small compared to the wavelength. Now using the ion continuity Eq. (2), we have

$$\partial_x (J_{Ox} + J_{Hx} + J_{sp,x}) = -\partial_t (en_O + en_H + en_{sp}). \quad (12)$$

Using Eqs. (12) and (11), Eq. (10) can be written as

$$\partial_x^2 \partial_z^2 (\phi - \psi) = \frac{4\pi}{c^2} \partial_t^2 (en_O + en_H + en_{sp}). \quad (13)$$

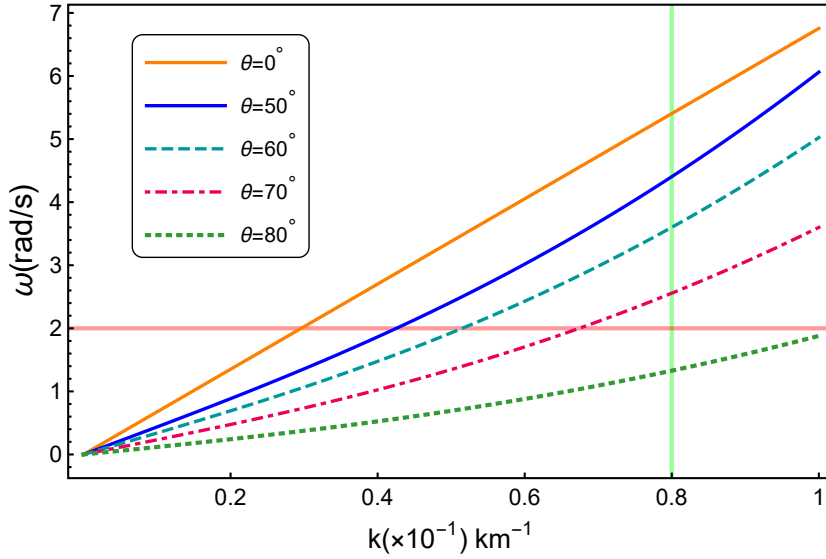


**Fig. 2.** Linear dispersion curves for KAWs propagating in the Venusian plasma for different angles with respect to the ambient magnetic field. Dispersion curves are shown for  $\theta = 0^\circ$  (orange),  $\theta = 50^\circ$  (blue),  $\theta = 60^\circ$  (dashed mint green),  $\theta = 70^\circ$  (dot-dashed pink), and  $\theta = 80^\circ$  (dotted green). Other plasma parameters:  $n_{O0} = 40 \text{ cm}^{-3}$ ,  $n_{H0} = 16 \text{ cm}^{-3}$ ,  $n_{sp0} = n_{se0} = 17 \text{ cm}^{-3}$ ,  $T_{se} = 15 \text{ eV}$ ,  $T_e = 10 \text{ eV}$ , and  $B_0 = 80 \times 10^{-5} \text{ G}$ .

### 2.3. Linear dispersion relation

The linear dispersion relation is obtained by linearizing the set of Eqs. (2), (3), (5), (6), and (13), applying a sinusoidal perturbation of the form  $\sim \exp[i(k_x x + k_z z - \omega t)]$  (where  $k_x$  and  $k_z$  are the perpendicular and parallel components of the wave vector, respectively, and  $\omega$  is the wave frequency). The dispersion relation is expressed as (see Appendix C for the details)

$$\omega^2 = k_z^2 v_{A0}^2 \left( 1 + \frac{(\gamma \rho_H^2 + \rho_O^2 + \delta \rho_{sp}^2) k_x^2}{(\alpha + \mu / \sigma_{se})} \right), \quad (14)$$

where we have defined the quantities

$$v_{A0} = \frac{B_0}{\sqrt{4\pi(n_{O0}m_O + n_{H0}m_H + n_{sp0}m_{sp})}},$$

$$\rho_i = \frac{C_{si}}{\Omega_i}, \quad C_{si} = \left( \frac{T_e}{m_i} \right)^{1/2}, \quad (15)$$

where  $v_{A0}$ ,  $\rho_i$ , and  $C_{si}$  represent the effective Alfvén speed, the ion-acoustic Larmor radius, and the ion-acoustic speed of the  $i$ th species, respectively. Also, we define the following ratios:

$$\gamma = \frac{n_{H0}}{n_{O0}}, \quad \delta = \frac{n_{sp0}}{n_{O0}}, \quad \alpha = \frac{n_{e0}}{n_{O0}}, \quad \mu = \frac{n_{se0}}{n_{O0}}, \quad \sigma_{se} = \frac{T_{se}}{T_e}. \quad (16)$$

We note here that the oxygen ion is taken as a reference because it has the highest density among other ionic species in this region at Venus. It is evident from Eq. (14) that the dispersion appears through the finite Larmor radius effects. Moreover, the dispersion is related to the concentration of both ionic species and electron populations. The greater the relative ion densities, the greater the dispersion associated with the perpendicular wavenumber. In the limiting case,  $(\gamma \rho_H^2 + \rho_O^2 + \delta \rho_{sp}^2) k_x^2 / (\alpha + \mu / \sigma_{se}) \ll 1$ , the dispersion relation (14) reduces to the dispersion relation of the non-dispersive shear Alfvén waves propagating in the plasma of the Venusian mantle (i.e.,  $\omega^2 = k_z^2 v_{A0}^2$ ).

In order to obtain some insight into the topology of the dispersion of KAWs, we can express the parallel and perpendicular

wavenumbers as  $k_z = k \cos \theta$  and  $k_x = k \sin \theta$  in terms of the angle  $\theta$  (where  $\theta$  is the angle between  $\mathbf{k}$  and  $\mathbf{B}_0$ ). For KAWs, we assume  $k_x \gg k_z$  (i.e.,  $\theta < \pi/2$ ). We plot the wave frequency  $\omega$  versus the wavenumber  $|\mathbf{k}|$ , as shown in Figs. 2–5, adopting real physical values found at the mantle region at Venus.

We note that, at  $\theta = 0^\circ$ , the MHD Alfvén mode is recovered, with  $\omega^2 = k_z^2 v_{A0}^2$ . Thus, the wave propagates parallel to the ambient magnetic field at phase velocity  $v_{A0}$ . On the other hand, at  $\theta = 90^\circ$  ( $k_z = 0$ ), the frequency vanishes ( $\omega = 0$ ) and the model breaks down. Therefore, we consider oblique propagation, assuming  $0^\circ < \theta < 90^\circ$ .

In the following, we use the particle and the magnetic field measurements carried out by both PVO and VEX to investigate the dispersion properties of the KAWs propagating in the ionosphere of Venus. The plasma parameters representative of the Venusian transition region are:  $n_{O0} = 30\text{--}50 \text{ cm}^{-3}$ ,  $n_{H0} = 15\text{--}17 \text{ cm}^{-3}$ ,  $n_{sp0} = 15\text{--}19 \text{ cm}^{-3}$ ,  $T_{se} = 10\text{--}30 \text{ eV}$ , and  $B_0 = 80\text{--}120 \times 10^{-5} \text{ G}$  (Lundin et al. 2011; Knudsen et al. 2016).

It is worth mentioning that KAWs are low-frequency waves, that is,  $\omega \ll \Omega_i$ . According to the plasma parameters mentioned above,  $\Omega_O \sim 0.5 \text{ rad s}^{-1}$  and  $\Omega_H = \Omega_{sp} \sim 8 \text{ rad s}^{-1}$ . Therefore, the frequency of the waves of interest should not exceed these values.

The effect of the angle of propagation is illustrated in Fig. 2: we see that the phase velocity decreases with increasing angle. Furthermore, at  $\theta = 0^\circ$  (i.e., parallel propagation), the wave becomes a nondispersive Alfvén wave with no kinetic effects. In this case, the phase velocity is at its highest value. We note that we did not take any angles below  $50^\circ$ , because these excitations arise when  $k_x \gg k_z$  (Baumjohann & Treumann 1996), which means  $\theta > 45^\circ$ . According to solar wind observations, only quasi-perpendicular KAWs dominate the observed spectrum, which may be because they are less damped than the less oblique KAWs (Sahraoui et al. 2012). Nevertheless, we still examine the less oblique waves because they are predicted by theory (see e.g., Hunana et al. 2013). To examine the effect of the angle on wave frequency, we calculate the frequency for different angles at fixed wavenumber (wavelength), and vice versa for its effect on wavelength. For example, at

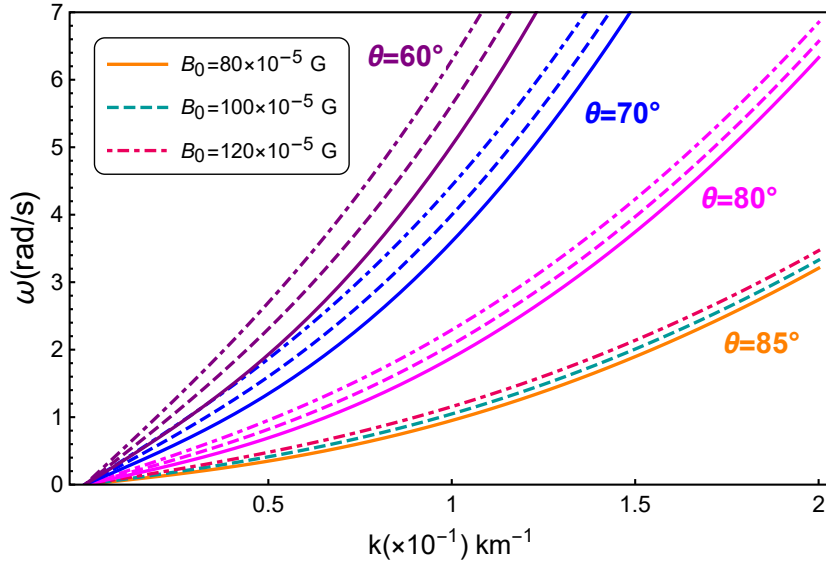


**Fig. 3.** Linear dispersion curves for KAWs propagating in the Venusian plasma for different values of ambient magnetic field and angles of propagation. The effect of the magnetic field is shown for  $B_0 = 80 \times 10^{-5}$  (orange),  $B_0 = 100 \times 10^{-5}$  (dashed mint green), and  $B_0 = 120 \times 10^{-5}$  (dot-dashed pink). Other plasma parameters:  $n_{O0} = 40 \text{ cm}^{-3}$ ,  $n_{H0} = 16 \text{ cm}^{-3}$ ,  $n_{sp0} = n_{se0} = 17 \text{ cm}^{-3}$ ,  $T_{se} = 15 \text{ eV}$ , and  $T_e = 10 \text{ eV}$ . The effect of the angle is shown for  $\theta = 85^\circ$  (multicolored curves),  $\theta = 80^\circ$  (magenta curves),  $\theta = 70^\circ$  (blue curves), and  $\theta = 60^\circ$  (purple curves). We note that all solid curves are for  $B_0 = 80 \times 10^{-5}$ , dashed curves are for  $B_0 = 100 \times 10^{-5}$ , and dot-dashed curves are for  $B_0 = 120 \times 10^{-5}$ . Moreover, multicolored curves are used for  $\theta = 85^\circ$  to easily distinguish between the curves for different magnetic field strength, which only show slight changes.

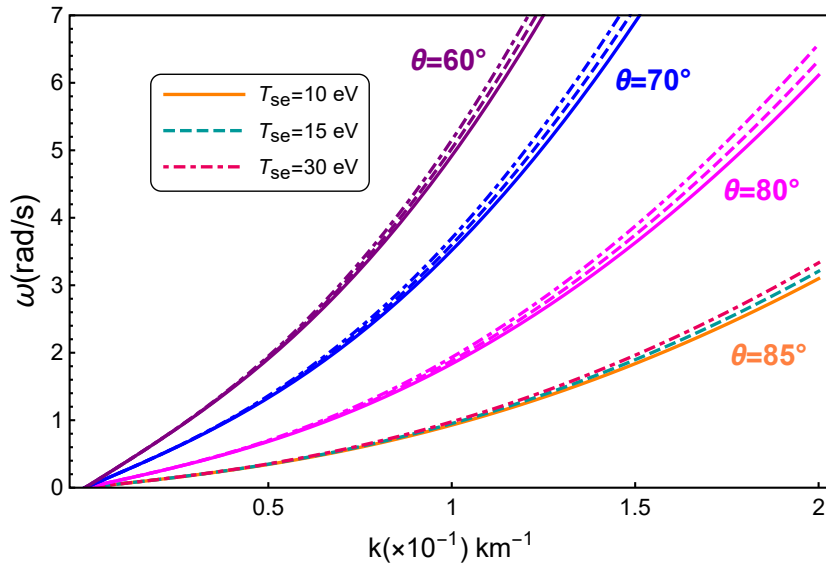


**Fig. 4.** Linear dispersion curves for KAWs propagating in the Venusian plasma for different values of solar wind electron temperature  $T_{se}$  and propagation angle. We show the effect of the solar wind electron temperature  $T_{se}$ , where  $T_{se} = 10 \text{ eV}$  (orange),  $T_{se} = 15 \text{ eV}$  (dashed mint green),  $T_{se} = 30 \text{ eV}$  (dot-dashed pink). Other plasma parameters:  $n_{O0} = 40 \text{ cm}^{-3}$ ,  $n_{H0} = 16 \text{ cm}^{-3}$ ,  $n_{sp0} = n_{se0} = 17 \text{ cm}^{-3}$ ,  $T_e = 10 \text{ eV}$ ,  $\theta = 85^\circ$ , and  $B_0 = 80 \times 10^{-5} \text{ G}$ . We also show the effect of angle, where  $\theta = 85^\circ$  (multicolored curves),  $\theta = 80^\circ$  (magenta curves),  $\theta = 70^\circ$  (blue curves), and  $\theta = 60^\circ$  (purple curves). We note that all solid curves are for  $T_{se} = 10 \text{ eV}$ , dashed curves are for  $T_{se} = 15 \text{ eV}$ , and dot-dashed curves are for  $T_{se} = 30 \text{ eV}$ . Moreover, multicolored curves are used for  $\theta = 85^\circ$  to easily distinguish between the curves, which show only slight changes.

$k = 0.8 \times 10^{-1} \text{ km}^{-1}$  ( $\lambda \sim 78 \text{ km}$ ), which is indicated by the green vertical line in Fig. 2, we take the intersection of the dispersion curves with this line to calculate the wave frequency for different angles. We find that the wave frequency for parallel propagation is  $f = 5.4 \text{ s}^{-1}$ , and it continues to decrease with increasing angle until it reaches  $f = 0.211 \text{ s}^{-1}$  for  $\theta = 80^\circ$ . On the other hand, for  $\omega = 2 \text{ rad s}^{-1}$  ( $f \sim 0.32 \text{ s}^{-1}$ ), which is indicated by the horizontal red line, the wavelength for  $\theta = 80^\circ$  is

$63 \text{ km}$ , and it continues to increase with decreasing angle until it reaches  $\lambda \sim 157 \text{ km}$  for  $\theta = 50^\circ$ .

The effect of the magnetic field with different angles is illustrated in Fig. 3: we can observe that the phase velocity is increasing with increasing magnetic field strength. This can be explained through the expression of the Alfvén speed  $v_{A0}$ , which indicates that the increase in magnetic field strength will increase the effective Alfvén speed, which in turn increases

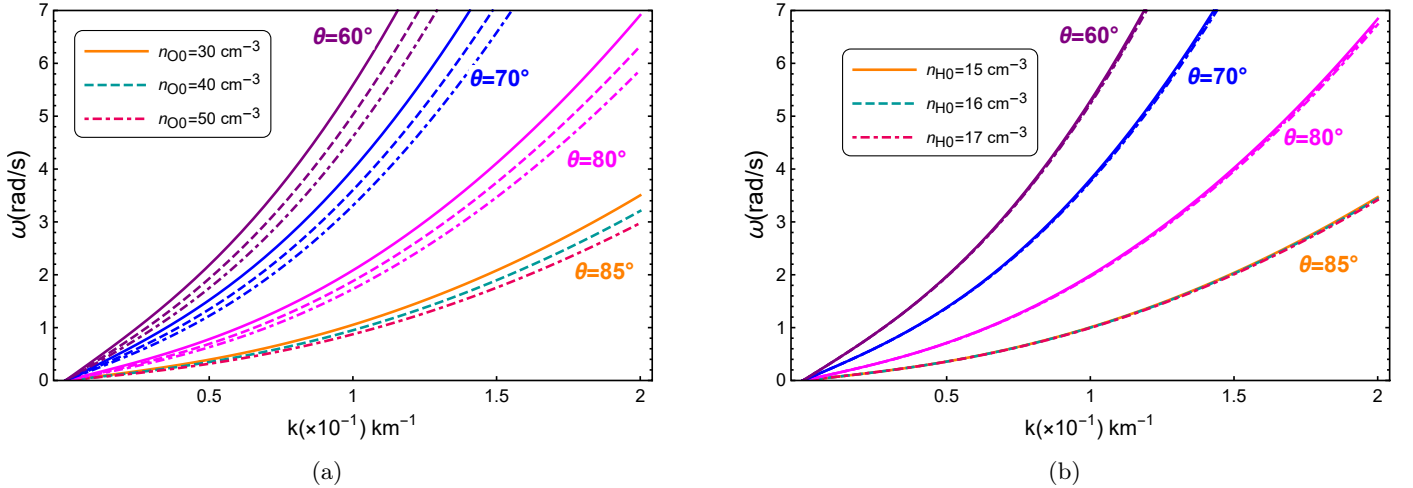


**Fig. 5.** Effect of ionic densities  $n_{O0}$  and  $n_{H0}$  and propagation angle on wave-phase velocity. (a) Effect of  $n_{O0}$ , where  $n_{O0} = 30 \text{ cm}^{-3}$  (orange),  $n_{O0} = 40 \text{ cm}^{-3}$  (dashed mint green), and  $n_{O0} = 50 \text{ cm}^{-3}$  (dot-dashed pink). (b) Effect of  $n_{H0}$ , where  $n_{H0} = 15 \text{ cm}^{-3}$  (dashed orange),  $n_{H0} = 16 \text{ cm}^{-3}$  (dashed mint green), and  $n_{H0} = 17 \text{ cm}^{-3}$  (dot-dashed pink). Other plasma parameters:  $n_{sp0} = n_{se0} = 17 \text{ cm}^{-3}$ ,  $T_e = 10 \text{ eV}$ , and  $B_0 = 80 \times 10^{-5} \text{ G}$ . We test the effects of the following propagation angles:  $\theta = 85^\circ$  (multicolored curves),  $\theta = 80^\circ$  (magenta curves),  $\theta = 70^\circ$  (blue curves), and  $\theta = 60^\circ$  (purple curves).

the wave phase velocity. As clearly shown in this figure, the magnetic field has a significant influence on the dispersion of KAWs at lower angles compared to higher ones. Furthermore, we observe that the phase velocity of the KAWs is increasing with decreasing propagation angle. We also note that the wavelength increases with decreasing propagation angle. For instance, for  $\omega \sim 3.7 \text{ rad s}^{-1}$  ( $f \sim 0.6 \text{ s}^{-1}$ ) and  $B_0 = 80 \times 10^{-5} \text{ G}$ , we obtain  $\lambda = 42, 61,$  and  $76 \text{ km}$  for  $\theta = 80, 70,$  and  $60^\circ$ , respectively.

The effect of solar wind electron temperature  $T_{se}$  is shown in Fig. 4. We note that the phase velocity is slightly increased by increasing  $T_{se}$  at higher wavenumber values. This is due to the fact that the parallel electric field is caused by the pressure of the electrons, and therefore hotter electrons enhance the parallel current, which in turn makes the KAWs move faster. On the contrary, colder electrons will slow the waves down. Moreover, the phase velocity increases with decreasing propagation angle. We also note that the solar wind electron temperature has a small influence on the dispersion of KAWs for all propagation angles.

The effect of ionic density is shown in Fig. 5. Evidently, increasing the oxygen ion concentration leads to a decrease in wave-phase velocity, which is in contrast to the hydrogen ions, which have a negligible effect on the wave-phase velocity, as illustrated in Fig. 5b. We observe that the influence of the oxygen ion density is enhanced for lower angles of propagation, in contrast to the hydrogen ions, which, regardless of the propagation angle, do not show any influence on the dispersion of KAWs. Solar wind protons have no effect on the wave-phase velocity, and so these are not discussed here. This can be explained physically through the expression of  $v_{A0}$ , which indicates that the increase in ionic equilibrium density will increase the ionic effective mass, resulting in a decrease in the effective Alfvén speed. Therefore, as lighter ions in the mantle region at Venus show only small density variations, they will have a negligible effect on the effective speed of Alfvén waves.

According to our linear analysis, we expect the small-amplitude KAWs propagating at the mantle region to have wavelengths of  $\sim 10\text{--}10^2 \text{ km}$  and a frequency range of  $\sim 10^{-2}$  up to  $\sim 5 \text{ Hz}$ .

#### 2.4. Nonlinear dynamics of kinetic Alfvén waves

The nonlinear dynamic set of equations of KAWs in normalized form reads as follows:

$$\partial_{\tilde{t}} \tilde{n}_H + \partial_{\tilde{x}} \tilde{n}_H \tilde{u}_{Hx} = 0, \quad (17)$$

$$\partial_{\tilde{t}} \tilde{n}_O + \partial_{\tilde{x}} \tilde{n}_O \tilde{u}_{Ox} = 0, \quad (18)$$

$$\partial_{\tilde{t}} \tilde{n}_{sp} + \partial_{\tilde{x}} \tilde{n}_{sp} \tilde{u}_{spx} = 0, \quad (19)$$

$$\tilde{u}_{Hx} = -\beta Q_H \partial_{\tilde{x}} \partial_{\tilde{t}} \tilde{\phi}, \quad (20)$$

$$\tilde{u}_{Ox} = -\beta \partial_{\tilde{x}} \partial_{\tilde{t}} \tilde{\phi}, \quad (21)$$

$$\tilde{u}_{spx} = -\beta Q_{sp} \partial_{\tilde{x}} \partial_{\tilde{t}} \tilde{\phi}, \quad (22)$$

$$\tilde{n}_e = \exp(\tilde{\psi}), \quad (23)$$

$$\tilde{n}_{se} = \exp(\tilde{\psi}/\sigma_{se}), \quad (24)$$

$$\partial_{\tilde{x}}^2 \partial_{\tilde{z}}^2 (\tilde{\phi} - \tilde{\psi}) = \frac{1}{\beta} \partial_{\tilde{t}}^2 (\gamma \tilde{n}_H + \tilde{n}_O + \delta \tilde{n}_{sp}), \quad (25)$$

$$\gamma \tilde{n}_H + \tilde{n}_O + \delta \tilde{n}_{sp} = \mu \tilde{n}_{se} + \alpha \tilde{n}_e. \quad (26)$$

The charge neutrality condition in equilibrium reads

$$\gamma + 1 + \delta = \mu + \alpha. \quad (27)$$

Here the time and space variables are normalized by the inverse of the oxygen cyclotron frequency  $\Omega_O^{-1} = (eB_0/m_Oc)^{-1}$ , and the oxygen ion inertial length  $\lambda_O = c/\omega_{pO}$ , respectively, where  $\omega_{pO} = (4\pi n_{O0} e^2/m_O)^{1/2}$  represents the oxygen ion plasma frequency. The densities  $n_j$  are normalized by the equilibrium number density  $n_{j0}$ , where  $j$  stands for  $O^+$ ,  $H^+$ ,  $sp^+$ ,  $e^-$ , and  $se^-$ . The fluid velocities of the ions  $u_{ix}$  are normalized by the oxygen Alfvén speed  $v_{AO} = B_0/\sqrt{4\pi n_{O0} m_O}$ . The potentials  $(\phi, \psi)$  are

normalized by  $T_e/e$ . The dimensionless parameter  $\beta = C_{so}^2/u_{AO}^2$  represents the plasma beta. Finally,  $Q_H(Q_{sp})$  denotes the mass ratio of the hydrogen ion (solar wind protons)  $m_H(m_{sp})$  to the oxygen ion  $m_O$ .

To study the obliquely propagating small-but-finite-amplitude kinetic Alfvén waves, we use the well-known reductive perturbation method (Washimi & Taniuti 1966) to transform the basic set of dynamic Eqs. (17)–(26) into one evolution equation. The stretching of independent variables is introduced in the standard fashion as follows:

$$\eta = \epsilon^{1/2}(l_x x + l_z z - u_0 t), \quad \tau = \epsilon^{1/2} t, \quad (28)$$

which gives  $\partial_x = \epsilon^{1/2} l_x \partial_\eta$ ,  $\partial_z = \epsilon^{1/2} l_z \partial_\eta$ , and  $\partial_t = \epsilon^{1/2}(\epsilon \partial_\tau - u_0 \partial_\eta)$ , where  $u_0$  is the normalized wave-phase velocity with respect to  $v_{AO}$ , which can be determined later. Here,  $l_x$  and  $l_z$  are the direction cosines in the  $x$ - and  $z$ -directions, respectively ( $l_x^2 + l_z^2 = 1$ ).

The perturbed quantities can be expanded as a power series of  $\epsilon$  about their equilibrium values as follows (Ghosh & Das 1994; Bandyopadhyay & Das 2000):

$$\begin{aligned} n_j &= 1 + \epsilon n_j^{(1)} + \epsilon^2 n_j^{(2)} + \dots \\ u_{ix} &= \epsilon u_{ix}^{(1)} + \epsilon^2 u_{ix}^{(2)} + \dots, \\ \psi &= \epsilon \psi^{(1)} + \epsilon^2 \psi^{(2)} + \dots, \\ \phi &= \phi^{(1)} + \epsilon \phi^{(2)} + \dots, \end{aligned} \quad (29)$$

where  $\epsilon$  is a small ( $0 < \epsilon < 1$ ) dimensionless expansion parameter representing the strength of nonlinearity. Due to the anisotropy introduced into the system by the magnetic field, the parallel and perpendicular potentials appear at different order in  $\epsilon$ . In other words, the wave affects the particles differently in the two directions.

Substituting Eqs. (28) and (29) into the set of nonlinear dynamic Eqs. (17)–(26), and collecting the lowest order in  $\epsilon$ , we have

$$\begin{aligned} -u_0 \partial_\eta n_H^{(1)} + l_x \partial_\eta u_{Hx}^{(1)} &= 0, \\ -u_0 \partial_\eta n_O^{(1)} + l_x \partial_\eta u_{Ox}^{(1)} &= 0, \\ -u_0 \partial_\eta n_{sp}^{(1)} + l_x \partial_\eta u_{spx}^{(1)} &= 0, \end{aligned} \quad (30)$$

$$\begin{aligned} u_{Hx}^{(1)} &= l_x \beta Q_H u_0 \partial_\eta^2 \phi^{(1)}, \\ u_{Ox}^{(1)} &= l_x \beta u_0 \partial_\eta^2 \phi^{(1)}, \\ u_{spx}^{(1)} &= l_x \beta Q_{sp} u_0 \partial_\eta^2 \phi^{(1)}, \end{aligned} \quad (31)$$

$$\begin{aligned} n_e^{(1)} &= \psi^{(1)}, \\ n_{se}^{(1)} &= \psi^{(1)} / \sigma_{se}, \end{aligned} \quad (32)$$

$$l_x^2 l_z^2 \partial_\eta^4 \phi^{(1)} = \frac{u_0^2}{\beta} \partial_\eta^2 (\gamma n_H^{(1)} + n_O^{(1)} + \delta n_{sp}^{(1)}). \quad (33)$$

The expression of the phase velocity is obtained by solving the lowest order Eqs. (30)–(33) for the KAWs:

$$u_0^2 = \pm \frac{l_z^2}{(1 + \gamma Q_H + \delta Q_{sp})}, \quad (34)$$

which is the normalized square of the wave-phase speed. It is clear that the phase velocity depends on the angle of propagation

as well as the ionic relative densities, but, on the other hand, the phase velocity is not affected by either the temperature or the concentration of electrons. In the following calculations, we take the positive value of  $u_0$ .

Now collecting the next order in terms of  $\epsilon$ , we have

$$\begin{aligned} \partial_\tau n_H^{(1)} - u_0 \partial_\eta n_H^{(2)} + l_x \partial_\eta u_{Hx}^{(1)} n_H^{(1)} + l_x \partial_\eta u_{Hx}^{(2)} &= 0, \\ \partial_\tau n_O^{(1)} - u_0 \partial_\eta n_O^{(2)} + l_x \partial_\eta u_{Ox}^{(1)} n_O^{(1)} + l_x \partial_\eta u_{Ox}^{(2)} &= 0, \\ \partial_\tau n_{sp}^{(1)} - u_0 \partial_\eta n_{sp}^{(2)} + l_x \partial_\eta u_{spx}^{(1)} n_{sp}^{(1)} + l_x \partial_\eta u_{spx}^{(2)} &= 0, \end{aligned} \quad (35)$$

$$\begin{aligned} u_{Hx}^{(2)} &= -\beta l_x Q_H \partial_\eta \partial_\tau \phi^{(1)} + \beta Q_H u_0 l_x \partial_\eta^2 \phi^{(2)}, \\ u_{Ox}^{(2)} &= -\beta l_x \partial_\eta \partial_\tau \phi^{(1)} + \beta u_0 l_x \partial_\eta^2 \phi^{(2)}, \\ u_{spx}^{(2)} &= -\beta l_x Q_{sp} \partial_\eta \partial_\tau \phi^{(1)} + \beta Q_{sp} u_0 l_x \partial_\eta^2 \phi^{(2)}, \end{aligned} \quad (36)$$

$$\begin{aligned} n_e^{(2)} &= \psi^{(2)} + \frac{1}{2} \psi^{(1)2}, \\ n_{se}^{(2)} &= \frac{\psi^{(2)}}{\sigma_{se}} + \frac{1}{2\sigma_{se}^2} \psi^{(1)2}, \end{aligned} \quad (37)$$

$$\gamma n_H^{(2)} + n_O^{(2)} + \delta n_{sp}^{(2)} = \mu n_{se}^{(2)} + \alpha n_e^{(2)}, \quad (38)$$

$$\begin{aligned} l_x^2 l_z^2 \partial_\eta^4 (\phi^{(2)} - \psi^{(1)}) &= \frac{1}{\beta} \left[ -2u_0 \partial_\tau \partial_\eta (\gamma n_H^{(1)} + n_O^{(1)} + \delta n_{sp}^{(1)}) \right. \\ &\quad \left. + u_0^2 \partial_\eta^2 (\gamma n_H^{(2)} + n_O^{(2)} + \delta n_{sp}^{(2)}) \right]. \end{aligned} \quad (39)$$

Eliminating the second-order quantities from Eqs. (35)–(39) with the aid of first-order equations and the expression of the phase velocity (34), and solving them for  $\psi^{(1)}$ , we obtain the following evolution equation:

$$\partial_\tau \psi^{(1)} + A \psi^{(1)} \partial_\eta \psi^{(1)} + B \partial_\eta^3 \psi^{(1)} = 0, \quad (40)$$

where the coefficients of nonlinearity and wave dispersion are given as

$$\begin{aligned} A &= -\left( \frac{\mu}{\sigma_{se}} + \alpha \right) (1 + \gamma Q_H + \delta Q_{sp})^{1/2} l_z, \\ B &= -\frac{1}{2} \frac{(1 + \gamma Q_H + \delta Q_{sp})^{1/2}}{(\mu/\sigma_{se}) + \alpha} l_x^2 l_z \beta. \end{aligned} \quad (41)$$

Equation (40) is known as the KdV equation, which describes the propagation of the nonlinear kinetic Alfvén waves during the interaction between the solar wind and the Venusian planetary plasma.

For the solitary wave solution of the KdV equation, we consider a frame  $\zeta = \eta - v_0 \tau$  moving with velocity  $v_0$  normalized by the Alfvén speed  $v_A$ , and impose the appropriate boundary conditions for the localized solution, that is,  $\psi \rightarrow 0$ ,  $d\psi/d\zeta \rightarrow 0$ , and  $d^2\psi/d\zeta^2 \rightarrow 0$  at  $\zeta = \pm\infty$ , which gives

$$\psi^{(1)} = \psi_0 \operatorname{sech}^2 \left( \frac{\zeta}{w} \right), \quad (42)$$

where the maximum potential perturbation (amplitude) and the spatial extension (width) of the solitary pulse are defined as  $\psi_0 = 3v_0/A$  and  $w = \sqrt{4B/v_0}$ , respectively. We note that the pulse amplitude is proportional to the solitary wave speed  $v_0$  while the width is inversely proportional to  $\sqrt{v_0}$ , signifying that faster pulses are taller and narrower while slower ones are shorter and broader. We also noted that the plasma beta  $\beta$  has no effect on the pulse amplitude as the nonlinear coefficient  $A$  is independent

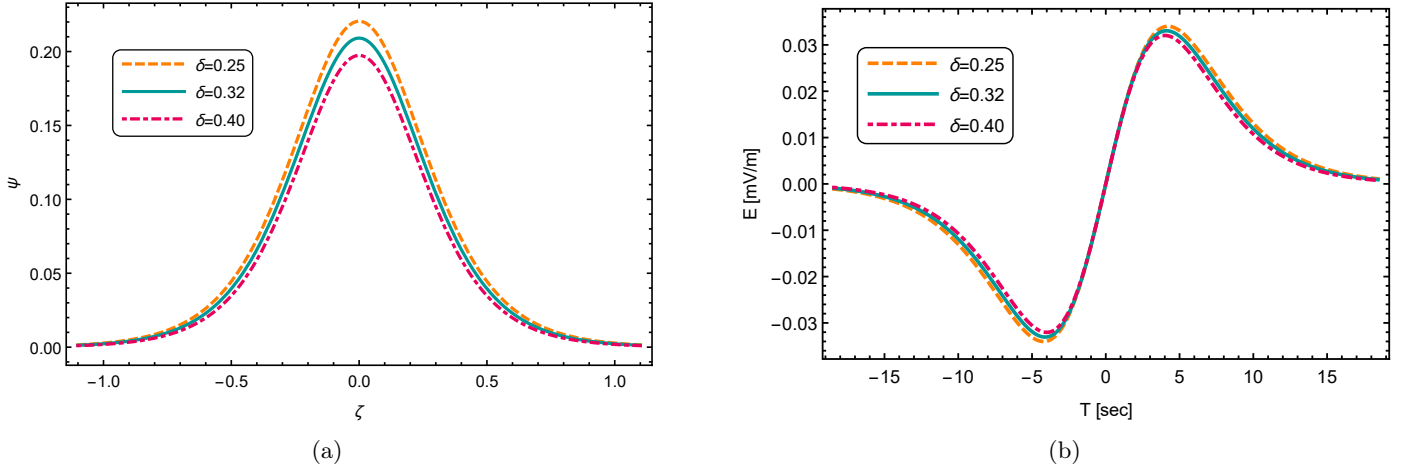


**Fig. 6.** Profiles of the solitary pulse and its corresponding electric field. (a) Solitary pulse versus  $\zeta$ . (b) Corresponding bipolar electric field for different values of  $\delta$ , where  $\delta = 0.25$  (dashed orange),  $\delta = 0.32$  (mint green), and  $\delta = 0.40$  (dot-dashed pink). Other plasma parameters are  $T_e = 10$  eV,  $B_0 = 100 \times 10^{-5}$  G,  $l_z (= \cos \theta) = 0.1$ ,  $\sigma_{se} = 2$ ,  $\mu = 0.32$ , and  $\gamma = 0.25$ .

of  $\beta$ . Here, we have a dispersion coefficient  $B < 0$ , and therefore to have positive values of the solitary pulse width,  $v_0$  must have negative values. Therefore,  $\zeta = \epsilon^{1/2}[l_x x + l_z z - (u_0 + \epsilon v_0)t]$ , which shows that kinetic Alfvén solitary pulses move with a speed of  $V = u_0 + \epsilon v_0$ , which is lower than the normalized phase speed of the wave in lab frame. The compressive structures of the KAWs are formed because the nonlinear coefficient  $A < 0$  and  $v_0 < 0$  must hold for real values of the width of the pulse, and its amplitude becomes positive.

### 3. Numerical results

In this study, we wish to illustrate how the KAWs are affected by the relevant conditions at the Venusan transition region. Our study is inspired by the measurements of both PVO and VEX missions. It is reported that the ionic loss starts at heights of  $\sim 300$ – $800$  km (Lundin 2011). As we are interested in the impact of the solar wind forcing on the KAWs characteristics, as well as the generation of the superthermal populations, we constructed our model at altitudes of 1000–2000 km, where a mixture of both planetary particles and solar wind particles is found. We anticipate that the parallel electric field produced by the KAWs is one mechanism by which charged particles are accelerated above the ionopause, which would contribute to the process of ionic loss at Venus. For this purpose, we use the observational data mentioned in Sect. 2.3 to calculate the dimensionless ratios representative of the Venusan mantle:  $\delta = (0.25-0.4)$ ,  $\mu = (0.25-0.40)$ ,  $\gamma = (0.20-0.30)$ ,  $\sigma_{se} = (1.00-3.00)$ , and  $B_0 = (85-120)$  nT (Lundin et al. 2011; Knudsen et al. 2016). We note that we calculated these parameters by varying the value of the numerator of the ratio while fixing the denominator (the reference value). For instance, increasing  $\sigma_{se}$  describes the increase in  $T_{se}$  while fixing  $T_e$ ; and increasing  $\gamma$  and  $\delta$  means that we increase  $n_{H0}$  and  $n_{sp0}$ , respectively, while fixing  $n_{O0}$ . We are using normalized quantities in this stage of our analysis for simplicity, and to show the reader how small changes affect the wave profile.

First, we investigate the effect of the ionic concentrations through the parameters  $\delta (= n_{sp0}/n_{O0})$  and  $\gamma (= n_{H0}/n_{O0})$  on both the solitary pulse profile and its associated bipolar electric field as illustrated in Figs. 6 and 7. As clearly shown, increasing  $\delta$  and  $\gamma$  slightly reduces the amplitude and width of the solitary

pulse along with the magnitude and duration of the corresponding electric field pulse. We expect that stronger parallel fields will build up at more tenuous regions at the Venusan environment, and this will lead to stronger energization of the planetary particles. At Venus, as we go up to higher altitudes, we find the plasma gets more tenuous (Lundin et al. 2011), and so it is expected that stronger parallel fields and acceleration events will occur at higher altitudes.

The influence of the relative temperature of electrons  $\sigma_{se} (= T_{se}/T_e)$  on the solitary pulse and its associated electric field is illustrated in Fig. 8, where we see that both the solitary pulse amplitude and the electric pulse magnitude are amplified with increasing  $\sigma_{se}$ . This is reasonable, because the parallel electric fields of the wave are sustained by the thermal pressure of the electrons. Therefore, the higher thermal pressure of the electrons leads to stronger parallel currents and parallel electric fields, and this is why taller solitary pulses are formed. In conditions with increased numbers of energetic solar wind electrons, we could expect stronger parallel electric fields to form at the mantle, which would provide a source of energization to the planetary particles.

The influence of the plasma  $\beta$  (via  $B_0$ ) is illustrated in Fig. 9. Increasing the magnetic field strength evidently has no effect on the pulse amplitude, but it forms narrower solitary pulses. On the contrary, it is shown that the electric pulse magnitude (duration) is significantly enhanced (decreased) with increasing  $B_0$ . According to Eq. (42), the maximum amplitude of the solitary pulse  $\psi_0$  is independent of the strength of the ambient magnetic field. The waveform of the electric pulse can be obtained from the expression  $E_{\parallel} = -\nabla\psi$ . The bipolar electric field is expressed as

$$E_{\parallel} = E_0 \text{Sech}^2\left(\frac{\zeta}{w}\right) \text{Tanh}\left(\frac{\zeta}{w}\right), \quad (43)$$

where  $E_0 = (\psi_0/w)$  is the maximum amplitude of the electric pulse. It is apparent that the maximum amplitude of the electric field is a function of the plasma  $\beta$  (and therefore the magnetic field). This explains why the magnitude of the electric pulse is sensitive to variation of  $B_0$ , in contrast to the amplitude of the solitary pulse. Accordingly, we expect that at conditions of lower  $\beta$  plasma, stronger electric fields will build up and therefore more acceleration bursts will occur at the Venusan transition region.

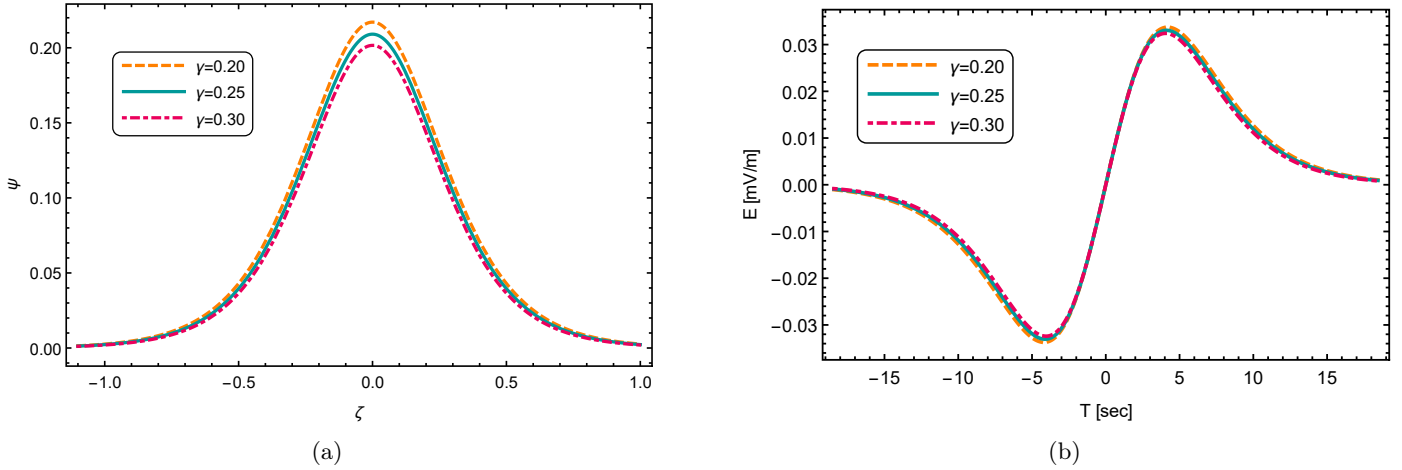


**Fig. 7.** Profiles of the solitary pulse and its corresponding electric field. (a) Solitary pulse versus  $\zeta$ . (b) Corresponding bipolar electric field for different values of  $\gamma$ , where  $\gamma = 0.20$  (dashed orange),  $\gamma = 0.25$  (mint green), and  $\gamma = 0.30$  (dot-dashed pink). Other plasma parameters are  $T_e = 10$  eV,  $B_0 = 100 \times 10^{-5}$  G,  $l_z (= \cos \theta) = 0.1$ ,  $\sigma_{se} = 2$ , and  $\mu = \delta = 0.32$ .

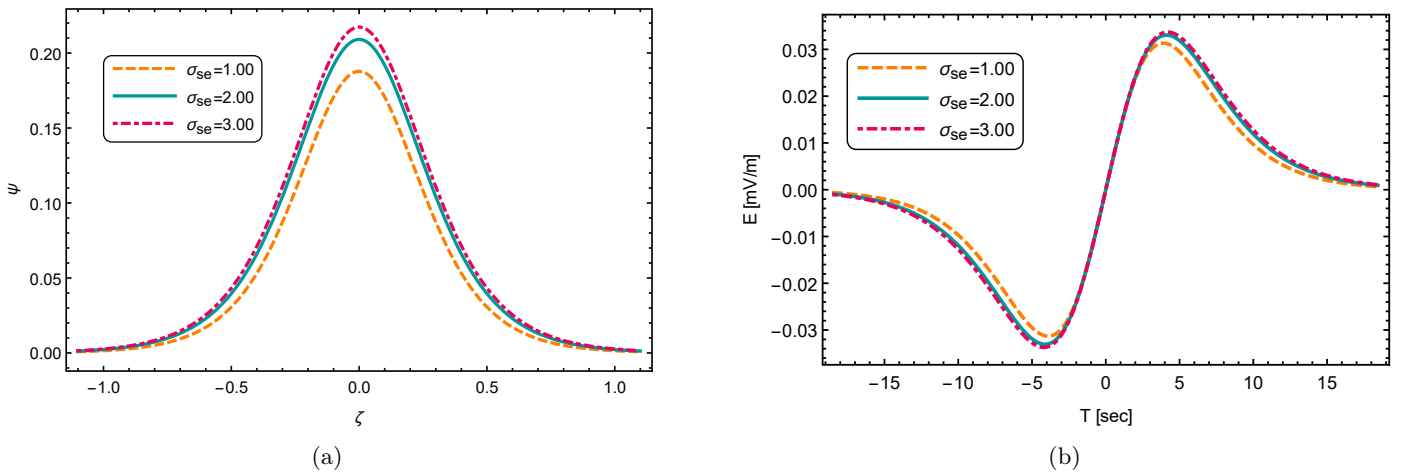


**Fig. 8.** Profiles of the solitary pulse and its corresponding electric field. (a) Solitary pulse versus  $\zeta$ . (b) Corresponding bipolar electric field for different values of  $\sigma_{se}$ , where  $\sigma_{se} = 1$  (dashed orange),  $\sigma_{se} = 2$  (mint green), and  $\sigma_{se} = 3$  (dot-dashed pink). Other plasma parameters are  $T_e = 10$  eV,  $B_0 = 100 \times 10^{-5}$  G,  $l_z (= \cos \theta) = 0.1$ ,  $\mu = \delta = 0.32$ , and  $\gamma = 0.25$ .

We note here that both components of the wave electric field can accelerate particles and contribute to the ionospheric loss. However, particles can only escape if the wave fields are strong enough to accelerate particles against gravity. For example, perpendicular fields can accelerate the particles to form upflows, but they will only escape if they gain velocity equal to or above the escape velocity; otherwise, they will return back to the planet (circulation; Lundin 2011). On the other hand, field-aligned electric fields are considered one of the most important and efficient mechanisms contributing to the outflows and escape of the particles, and were reported to be associated with plasma depletion regions in the terrestrial environment and Venus (Grebowksy & Curtis 1981). This is because they aid the particles to overshoot along the draped magnetic field lines until they reach behind the planet and escape through the magnetotail (see Fig. 1). The magnetotail is considered one of the main escape channels at Venus, where particles can be accelerated again by other mechanisms (Grebowksy & Curtis 1981; Brace et al. 1987; Dubinin et al. 2012; Lundin 2011). In other words, particles reaching the tail region are more likely to escape. For this reason, we pay more attention to the parallel electric field of the wave.

The influence of the obliqueness parameter  $l_z$  is depicted in Fig. 10, where we see that the amplitude of the pulse increases with decreasing  $l_z$ , as the nonlinear coefficient  $A \propto l_z$ ,  $A$  will decrease with increasing obliqueness angle  $\theta$ . In other words, the solitary pulse becomes more spiky as it propagates more obliquely with respect to the magnetic field. We note that  $A$  vanishes for  $l_z = 0$ , that is, perpendicular to the magnetic field, and therefore no solitary waves are formed in this direction. For vanishing nonlinear effect (as the propagation angle increases), the solitary wave amplitude grows until the reductive perturbation technique is no longer valid, and the fully nonlinear effects should be taken into account. It is important to note that the width  $w \propto \sqrt{l_z^2} = \sqrt{\sin^2 \theta \cos \theta}$ , meaning that the width vanishes when  $l_z = 0$  ( $\theta = 90^\circ$ ) or  $l_z = 1$  ( $\theta = 0^\circ$ ), which means the hydrodynamic model is no longer valid in the direction parallel to the magnetic field and the wave turns to the nondispersive MHD Alfvén mode. Therefore, no solitary pulses can form in directions that are either exactly parallel or perpendicular to the magnetic field.

Finally, the outcomes of our work suggest the excitation of elliptically polarized (Cramer 2011) solitary kinetic Alfvén structures that can produce ultralow-frequency (ULF) activity

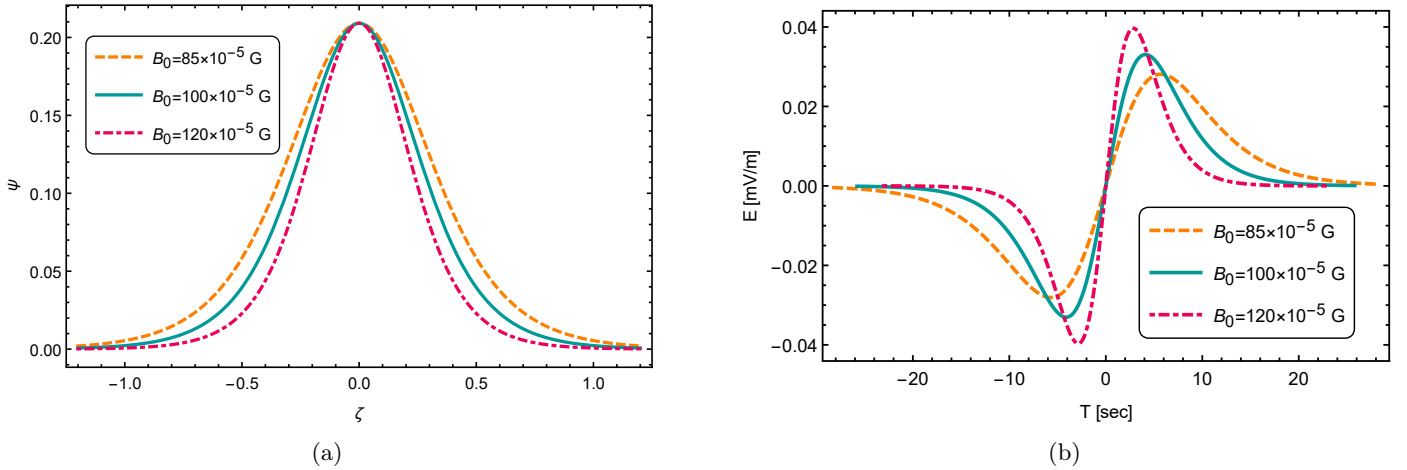


**Fig. 9.** Profiles of the solitary pulse and its corresponding electric field. (a) Solitary pulse versus  $\zeta$ . (b) Corresponding bipolar electric field for different values of  $B_0$ , where  $B_0 = 85 \times 10^{-5}$  G (dashed orange),  $B_0 = 100 \times 10^{-5}$  G (mint green), and  $B_0 = 120 \times 10^{-5}$  G (dot-dashed pink). Other plasma parameters are  $T_e = 10$  eV,  $l_z (= \cos \theta) = 0.1$ ,  $\sigma_{se} = 2$ ,  $\mu = \delta = 0.32$ , and  $\gamma = 0.25$ .

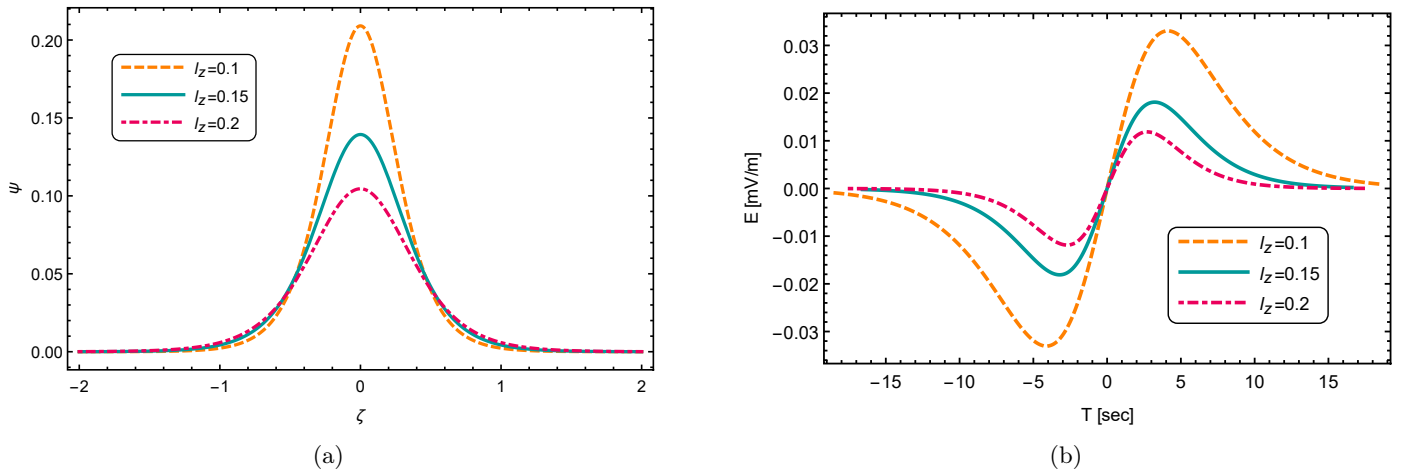


**Fig. 10.** Profiles of the solitary pulse and its corresponding electric field. (a) Solitary pulse versus  $\zeta$ . (b) Corresponding bipolar electric field for different values of  $l_z (= \cos \theta)$ , where  $l_z = 0.1$  (dashed orange),  $l_z = 0.15$  (mint green), and  $l_z = 0.2$  (dot-dashed pink). Other plasma parameters are  $T_e = 10$  eV,  $B_0 = 85 \times 10^{-5}$  G,  $\sigma_{se} = 2$ ,  $\mu = \delta = 0.32$ , and  $\gamma = 0.25$ .

above the Venusian ionopause. Furthermore, by analogy to terrestrial observations, we expect that kinetic Alfvén waves may be associated with the observations of ionospheric cavities or depletion regions with enhanced electric fields and field-aligned currents (Wahlund et al. 1994; Seyler et al. 1995; Stasiewicz et al. 1997; Knudsen & Wahlund 1998). To estimate the range of frequencies produced by this wave, we carried out a Fast Fourier transform (FFT) analysis of the electric pulses that resulted from our numerical analysis, as shown in Fig. 11. Figures 11a,b show the amplitude of the pulse and the associated ambipolar electric field with variation of the directional cosine  $l_z$ . We find that the maximum amplitude of the corresponding parallel electric field ranges from  $\sim 0.01$  to  $0.034$  mV m $^{-1}$  with a duration of  $\sim 20$ – $30$  s. Furthermore, the output of the FFT power spectrum of the E-field pulse (see Fig. 11c) is an electromagnetic noise in the frequency range of  $\sim 0.1$ – $1.6$  Hz and the peak occurs at the inverse of the pulse time duration  $\tau^{-1}$ , where the frequency peak is found to be around  $\sim 0.177$  Hz.

#### 4. Conclusions

In this work, we propose a mechanism for accelerating charged particles through the parallel electric fields of the KAWs at the

upper atmosphere of Venus. For this purpose, we constructed a plasma model to investigate the linear and nonlinear dynamics of the KAWs propagating in a plasma inspired by the plasma found at the Venusian transition zone. We traced the influence of the ionic concentrations, the obliqueness, the magnetic field strength, and the temperature of the electrons to the basic features of the linear and nonlinear KAWs and their corresponding parallel electric field. A linear analysis illustrates that the phase velocity of the KAWs is sensitive to both the propagation angle and the equilibrium density of the oxygen ion population, where lower propagation angles and denser oxygen populations of ionospheric origin are found to increase the wave phase velocity. We also predict that KAWs could reach wavelengths of  $\sim 10$ – $10^2$  km, while the frequency starts from  $\sim 10^{-2}$  up to  $\sim 5$  Hz. We find that our model predicts only compressive pulses with sub-Alfvénic speeds in the lab frame. Moreover, we find that a higher temperature ratio, a stronger magnetic field, and larger propagation angles are enhancing the parallel ambipolar field, while denser ionic concentration leads to a slightly diminished electric field magnitude. The FFT analysis of the parallel electric field of KAWs predicts ULF solitary kinetic Alfvénic excitations with durations of 20–30 s, an electric field magnitude of  $\sim 0.01$ – $0.034$  mV m $^{-1}$ , and a frequency range of  $\sim 0.1$ – $1.6$  Hz.

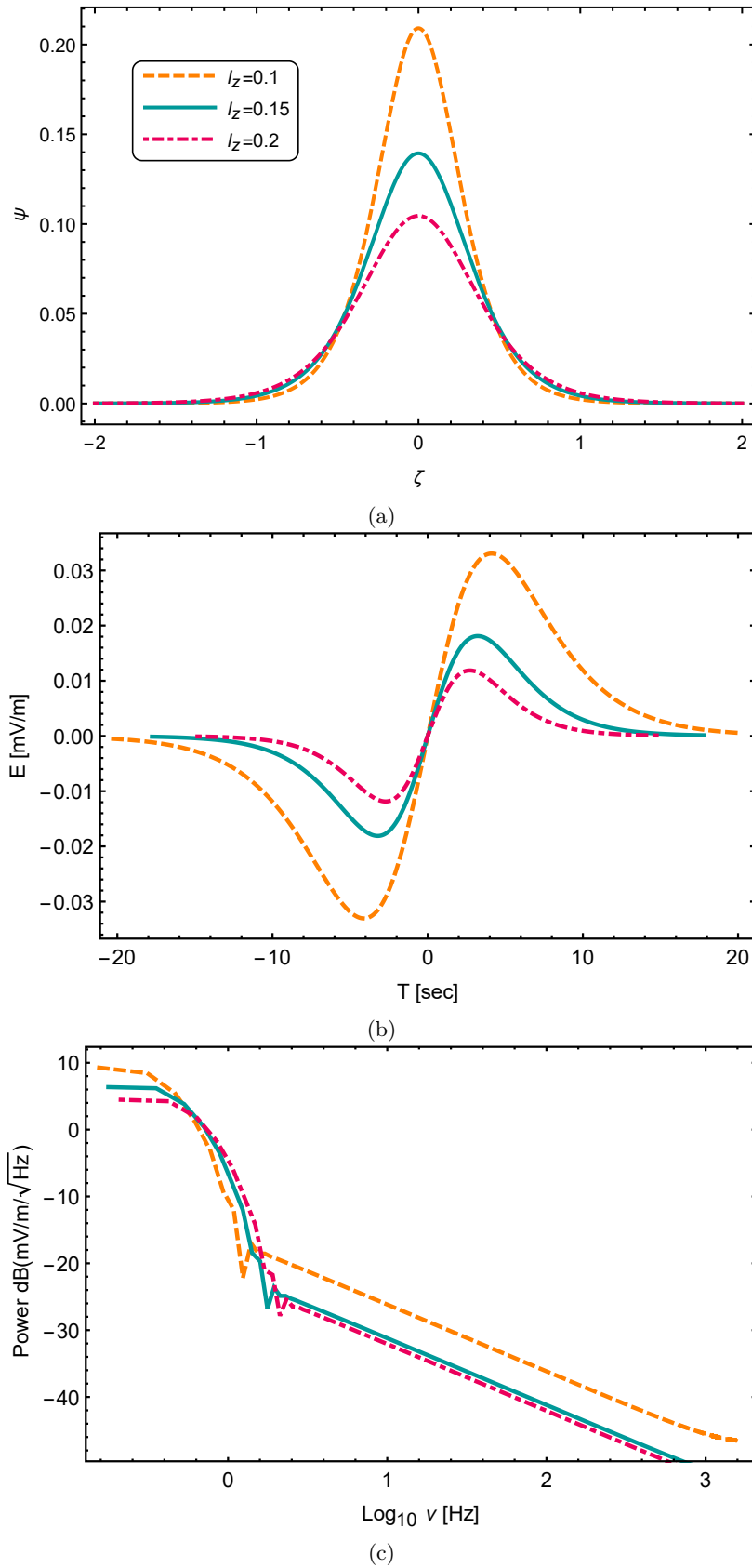


**Fig. 11.** Solitary wave profile with its corresponding electric field and FFT power spectra. (a) Solitary profiles versus  $\zeta$ . (b) Corresponding bipolar electric field for different values of  $l_z$  where  $l_z = 0.1$  (dashed orange),  $l_z = 0.15$  (mint green), and  $l_z = 0.2$  (dot-dashed pink). (c) Corresponding FFT power spectra of the electric fields. The  $x$ -axis represents the  $\log_{10} \nu$  where  $\nu$  is the frequency in Hz and the  $y$ -axis resembles the power of the electric field expressed in units of decibels  $\text{dB}(mV/v/\sqrt{\text{Hz}})$  with frequency peaks at  $f_p = 0.155$  Hz (dashed orange),  $f_p = 0.177$  Hz (mint green), and  $f_p = 0.212$  Hz (dot-dashed pink).

Our study may be beneficial in detecting these structures at the Venusian upper atmosphere by future missions. KAWs are not observed yet at Venus. In principle, this may be caused by the lack of instrumentation on board previous missions. For instance, PVO had a magnetometer and an electric field sensor; both were capable of measuring the magnetic and electric fields fluctuations. However, unfortunately, both instruments were not synchronized, which led to an ambiguity in characterizing the observed fluctuations. On the other hand, VEX had a magnetometer only, which can detect the fluctuating magnetic fields. Consequently, these restrictions do not allow us to conclude on whether or not KAWs exist. Fränz et al. (2017) reported the existence of ULF wave activity consisting of Alfvénic waves, mirror modes, and slow and fast modes in the solar wind and the magnetosheath. These authors combined the magnetic field measurements and the particle observations carried out by VEX to gather more information about the detected modes in order to identify them. Although they were able to identify various Alfvénic modes by calculating different parameters, such as the compressibility, angle of propagation, and amplitude, those are not indications for KAWs; this is why we believe that KAWs produce almost no compressions in the magnetic field. In order to identify these waves, magnetic field and particle observations should be carried out that coincide with electric field measurements. Furthermore, we conclude that future missions need to be equipped with high-performance instruments able to measure electromagnetic fluctuations and capable of characterizing a broad spectrum of wave modes.

*Acknowledgements.* The authors acknowledge the sponsorship provided by the Alexander von Humboldt Stiftung (Bonn, Germany) in the framework of the Research Group Linkage Programme funded by the respective Federal Ministry. M.L. acknowledges support from the Ruhr-University Bochum and the Katholieke Universiteit Leuven. These results were also obtained in the framework of the projects G.0025.23N (FWO-Vlaanderen) and SIDC Data Exploitation (ESA Prodex-12). A. A. Fayad would like to thank I. S. Elkamash for the useful discussions.

## References

- Afify, M. S., Elkamash, I. S., Shihab, M., & Moslem, W. M. 2021, *Adv. Space Res.*, **67**, 4110
- Bandyopadhyay, A., & Das, K. 2000, *Phys. Plasmas*, **7**, 3227
- Baumjohann, W., & Treumann, R. A. 1996, *Basic Space Plasma Physics* (London: Imperial College Press)
- Bellan, P. M. 2008, *Fundamentals of Plasma Physics* (Cambridge University Press)
- Brace, L., & Kliore, A. 1991, *Space Sci. Rev.*, **55**, 81
- Brace, L., Kasprzak, W., Taylor, H., et al. 1987, *J. Geophys. Res. Space Phys.*, **92**, 15
- Chaston, C., Génot, V., Bonnell, J., et al. 2006, *J. Geophys. Res. Space Phys.*, **111**
- Coates, A. 2004, *Adv. Space Res.*, **33**, 1977
- Colin, L. 1980, *JGR Space Phys.*, **85**, 7575
- Cramer, N. F. 2011, *The Physics of Alfvén Waves* (John Wiley & Sons)
- Curtis, S., Brace, L., & Kasprzak, W. 1981, in *International Conference on the Venus Environment*, NASA/Ames Res. Cent., Mountain View, Calif
- Dubinin, E., Fraenz, M., Fedorov, A., et al. 2011, in *The Plasma Environment of VENUS, Mars, and Titan* (Springer), 173
- Dubinin, E., Fraenz, M., Fedorov, A., et al. 2012, *The Plasma Environment of Venus, Mars, and Titan* (Springer), 173
- Dubinin, E., Luhmann, J. G., & Slavin, J. A. 2020, *Oxford Research Encyclopedia of Planetary Science* (Oxford University Press), 1
- Fränz, M., Echer, E., De Souza, A. M., Dubinin, E., & Zhang, T. 2017, *Planet. Space Sci.*, **146**, 55
- Futaana, Y., Stenberg Wieser, G., Barabash, S., & Luhmann, J. G. 2017, *Space Sci. Rev.*, **212**, 1453
- Gary, S. P. 1986, *J. Plasma Phys.*, **35**, 431
- Ghosh, G., & Das, K. 1994, *J. Plasma Phys.*, **51**, 95
- Grebowsky, J., & Curtis, S. 1981, *Geophys. Res. Lett.*, **8**, 1273
- Grebowsky, J., Kasprzak, W., Hartle, R., Mahajan, K., & Wagner, T. 1993, *J. Geophys. Res. Planets*, **98**, 9055
- Hasegawa, A., & Mima, K. 1976, *Phys. Rev. Lett.*, **37**, 690
- Hasegawa, A., & Uberoi, C. 1982, Alfvén wave, DOE Critical Review Series
- Hunana, P., Goldstein, M., Passot, T., et al. 2013, *ApJ*, **766**, 93
- Jarvinen, R., Brain, D., & Luhmann, J. 2016, *Planet. Space Sci.*, **127**, 1
- Jarvinen, R., Kallio, E., Janhunen, P., et al. 2009, *Annales Geophysicae*, **27**, 4333
- Kadomtsev, B. B. 1956, *Plasma Turbulence* (Academic Press), 82
- Kasprzak, W., Taylor, H., Brace, L., Niemann, H., & Scarf, F. 1982, *Planet. Space Sci.*, **30**, 1107
- Knudsen, D. J., & Wahlund, J.-E. 1998, *J. Geophys. Res. Space Phys.*, **103**, 4157
- Knudsen, W. C., Jones, D. E., Peterson, B. G., & Knadler Jr., C. E. 2016, *J. Geophys. Res. Space Phys.*, **121**, 7753
- Lundin, R. 2011, *The Plasma Environment of Venus, Mars, and Titan* (Springer), 309
- Lundin, R., Barabash, S., Futaana, Y., et al. 2011, *Icarus*, **215**, 751
- Martinez, C., Boeswetter, A., Fränz, M., et al. 2009, *J. Geophys. Res. Planets*, **114**, E9
- Moslem, W., Elsheikh, I., Tolba, R., El-Zant, A., & El-Metwally, M. 2021, *Adv. Space Res.*, **68**, 1525
- Pérez-de Tejada, H., & Lundin, R. 2023, <https://doi.org/10.5772/intechopen.109039>
- Phillips, J. L., & McComas, D. J. 1991, *Space Sci. Rev.*, **55**, 1
- Sahraoui, F., Belmont, G., & Goldstein, M. 2012, *ApJ*, **748**, 100
- Salem, S., Moslem, W., Lazar, M., et al. 2020, *Adv. Space Res.*, **65**, 129
- Seyler, C., Wahlund, J.-E., & Holback, B. 1995, *J. Geophys. Res. Space Phys.*, **100**, 21453
- Spenner, K., Knudsen, W. C., Miller, K. L., et al. 1980, *J. Geophys. Res. Space Phys.*, **85**, 7655
- Stasiewicz, K., Gustafsson, G., Marklund, G., et al. 1997, *J. Geophys. Res. Space Phys.*, **102**, 2565
- Svedhem, H., Titov, D. V., McCoy, D., et al. 2007, *Planet Space Sci*, **55**, 1636
- Szegö, K., Shapiro, V., Shevchenko, V., et al. 1991, *Geophys. Res. Lett.*, **18**, 2305
- Taylor, H., Brinton, H., Wagner, T., Blackwell, B., & Cordier, G. 1980a, *IEEE Trans. Geosci. Remote Sensing*, **GE-18**, 44
- Taylor Jr, H., Brinton, H., Bauer, S., et al. 1980b, *J. Geophys. Res. Space Phys.*, **85**, 7765
- Taylor Jr, H., Daniell, R., Hartle, R., et al. 1981, *Adv. Space Res.*, **1**, 247
- Terada, N., Shinagawa, H., & Machida, S. 2004, *Adv. Space Res.*, **33**, 161
- Titov, D. V., Svedhem, H., Koschny, D., et al. 2006, *Planet Space Sci.*, **54**, 1279
- Wahlund, J.-E., Louarn, P., Chust, T., et al. 1994, *Geophys. Res. Lett.*, **21**, 1831
- Washimi, H., & Taniuti, T. 1966, *Phys. Rev. Lett.*, **17**, 996

## Appendix A: Nomenclature

$e$	electron charge
$c$	speed of light
$k_B$	Boltzmann constant
$m_j$	mass of the $j$ th species
$n_j$	density of the $j$ th species
$n_{j0}$	the equilibrium density of the $j$ th species
$T_j$	temperature of the $j$ th species
$\rho_i$	the ion Larmor radius
$\Omega_i$	the ion cyclotron frequency
$\beta$	plasma beta
$\mathbf{E}$	wave electric field
$\mathbf{B}$	the magnetic field
$\mathbf{B}_0$	the local magnetic field
$\phi$	electrostatic potential
$\psi$	electromagnetic potential
$\mathbf{A}$	vector potential
$\mathbf{u}_i$	ion fluid velocity
$\mathbf{J}$	current density
$\omega$	the wave frequency
$\mathbf{k}$	the wave vector
$\lambda$	the wavelength
$k_x$	perpendicular wavenumber
$k_z$	parallel wavenumber
$v_{A0}$	effective Alfvén speed
$C_{si}$	ion-acoustic speed
$\gamma$	density ratio of $n_{H0}$ over $n_{O0}$
$\delta$	density ratio of $n_{sp0}$ over $n_{O0}$
$\alpha$	the density ratio of $n_{e0}$ over $n_{O0}$
$\mu$	the density ratio of $n_{se0}$ over $n_{O0}$
$\sigma_{se}$	the temperature ratio of $T_{se}$ over $T_e$
$\theta$	propagation angle
$\lambda_O$	oxygen ion inertial length
$Q_{H(sp)}$	the mass ratio of $m_H(m_{sp})$ over $m_O$
$\eta$	normalized space coordinate
$\tau$	normalized time coordinate
$\epsilon$	nonlinearity parameter
$l_{x,z}$	directional cosine in the $x$ - and $z$ -directions
$u_0$	normalized phase speed
$A$	nonlinearity coefficient
$B$	dispersion coefficient
$\zeta$	travelling wave transformation
$v_0$	frame velocity
$w$	soliton width
$\psi_0$	soliton amplitude
$E_{\parallel}$	bipolar electric field

## Appendix B: Derivation of the ion fluid velocity

For the case of low beta plasma, the momentum equation is written as

$$(\partial_t \mathbf{u}_i + (\mathbf{u}_i \cdot \nabla) \mathbf{u}_i) = \frac{e}{m_i} (\mathbf{E} + \frac{1}{c} \mathbf{u}_i \times \mathbf{B}_0). \quad (\text{B.1})$$

For motion perpendicular to the ambient magnetic field  $\mathbf{B}_0$ , we can neglect the convective term  $(\mathbf{u}_i \cdot \nabla) \mathbf{u}_i$  in the equation of motion, and it becomes

$$\partial_t \mathbf{u}_i = \frac{e}{m_i} (\mathbf{E} + \frac{1}{c} \mathbf{u}_i \times \mathbf{B}_0), \quad (\text{B.2})$$

$$\partial_t \mathbf{u}_i \times \mathbf{B}_0 = \frac{e}{m_i} [\mathbf{E} \times \mathbf{B}_0 + \frac{1}{c} (\mathbf{u}_i \times \mathbf{B}_0) \times \mathbf{B}_0], \quad (\text{B.3})$$

and the x-component of equation (B.3) is

$$\partial_t (u_{iy} B_0) = \frac{e}{m_i} E_y B_0 - \frac{e}{m_i c} u_{ix} B_0^2. \quad (\text{B.4})$$

As we know that  $E_y = 0$ , and we assume infinite conductivity (Hasegawa & Uberoi 1982),

$$\mathbf{E} + \frac{1}{c} \mathbf{u}_i \times \mathbf{B} = 0, \quad (\text{B.5})$$

$$E_x + \frac{1}{c} u_{iy} B_0 = 0, \quad (\text{B.6})$$

$$\frac{1}{c} u_{iy} B_0 = \partial_x \phi. \quad (\text{B.7})$$

Substituting equation (B.7) in equation (B.4), we get

$$u_{ix} = -\frac{m_i c^2}{e B_0^2} \partial_x \partial_t \phi, \quad (\text{B.8})$$

which is equation (3) in Sect. (2).

## Appendix C: Derivation of the dispersion relation

The linearization of equations (2), (3), (5), (6), and (13) along with the quasi-neutrality condition is performed by assuming the following linearization scheme:  $n_j = n_{j0} + n_{j1}$ ,  $u_{ix} = u_{ix1}$ ,  $\phi = \phi_1$ , and  $\psi = \psi_1$ . Here, the quantities with index ‘0’ represent the equilibrium value of that quantity, while the quantities with the index ‘1’ represent its first-order fluctuation. Thus, after the linearization of the basic set of dynamic equations and assuming all the first-order fluctuations to be of the form  $A = A \exp[i(k_x x + k_z z - \omega t)]$ , we obtain the following set of equations:

$$n_{i1} = \frac{k_x}{\omega} n_{i0} u_{ix1}, \quad (\text{C.1})$$

$$u_{ix1} = -\frac{c}{B_0 \Omega_{ic}} k_x \omega \phi_1, \quad (\text{C.2})$$

$$n_{e1} = n_{e0} \frac{e \psi_1}{T_e}, \quad n_{se1} = n_{se0} \frac{e \psi_1}{T_{se}}, \quad (\text{C.3})$$

$$n_{H1} + n_{O1} + n_{sp1} = n_{se1} + n_{e1}, \quad (\text{C.4})$$

and

$$k_x^2 k_z^2 (\phi_1 - \psi_1) = -\frac{4\pi e}{c^2} \omega^2 (n_{H1} + n_{O1} + n_{sp1}). \quad (\text{C.5})$$

Substituting (C.2) in (C.1), we get

$$n_{i1} = -k_x^2 \frac{n_{i0} c}{B_0 \Omega_{ic}} \phi_1. \quad (\text{C.6})$$

Substituting (C.6) and (C.3) in (C.4), we get

$$\phi_1 = -\frac{(\alpha + \mu / \sigma_{se})}{(\gamma \rho_H^2 + \rho_O^2 + \delta \rho_{sp}^2) k_x^2} \psi_1. \quad (\text{C.7})$$

Substituting (C.3), (C.6), and (C.7) in (C.5), we get the required linear dispersion relation of the kinetic Alfvén waves:

$$\omega^2 = k_z^2 v_{A0}^2 \left( 1 + \frac{(\gamma \rho_H^2 + \rho_O^2 + \delta \rho_{sp}^2) k_x^2}{(\alpha + \mu / \sigma_{se})} \right). \quad (\text{C.8})$$